Fermi National Accelerator Laboratory

FERMILAB-Pub-95/058-E

E789

Measurement of J/ψ and ψ' Production in 800 GeV/c Proton-Gold Collisions

M.H. Schub et al.
The E789 Collaboration

Fermi National Accelerator Laboratory
P.O. Box 500, Batavia, Illinois 60510

March 1995

Submitted to *Physical Review D*

Operated by Universities Research Association Inc. under Contract No. DE-AC02-76CHO3000 with the United States Department of Energy

Disclaimer

Measurement of J/ψ and ψ' Production in 800 GeV/c Proton-Gold Collisions

M. H. Schub,[1,a] D. M. Jansen,[2] C. S. Mishra,[3] P. M. Ho,[4] C. N. Brown,[3] T. A. Carey,[2] Y. C. Chen,[5,b] R. Childers,[6] W. E. Cooper,[3] C. W. Darden,[6] G. Gidal,[4] K. N. Gounder,[3,c] L. D. Isenhower,[7] R. G. Jeppesen,[2,d] D. M. Kaplan,[8,e] J. S. Kapustinsky,[2] G. C. Kiang,[9] M. S. Kowitt,[4,f] D. W. Lane,[2,g] L. M. Lederman,[1,e] M. J. Leitch,[2] J. W. Lillberg,[2] W. R. Luebke,[8,e] K. B. Luk,[4] P. L. McGaughey,[2] J. M. Moss,[2] J. C. Peng,[2] R. S. Preston,[8] D. Pripstein,[4] J. Sa,[8] M. E. Sadler,[7] R. Schnathorst,[7] V. Tanikella,[8] P. K. Teng,[9] J. R. Wilson[6]

[1] *University of Chicago, Chicago, IL 60637*
[2] *Los Alamos National Laboratory, Los Alamos, NM 87545*
[3] *Fermi National Accelerator Laboratory, Batavia, IL 60510*
[4] *Lawrence Berkeley Laboratory and University of California, Berkeley, CA 94720*
[5] *National Cheng Kung University, Tainan, Taiwan, R.O.C.*
[6] *University of South Carolina, Columbia, SC 29208*
[7] *Abilene Christian University, Abilene, TX 79699*
[8] *Northern Illinois University, DeKalb, IL 60115*
[9] *Institute of Physics, Academia Sinica, Taipei, Taiwan, R.O.C.*

(March 28, 1995)

Abstract

With a data sample containing 1.1×10^5 $J/\psi \to \mu^+\mu^-$ decays reconstructed with 16 MeV/c^2 rms mass resolution, we have measured the differential cross sections versus Feynman-x, rapidity, and p_T for the production of J/ψ and ψ' in 800 GeV/c p-Au collisions. Our results are compared with leading-order QCD predictions and with previous measurements. Assuming an appropriate form for the differential cross sections in regions not measured, we derive a total J/ψ production cross section $\sigma(p + N \to J/\psi + X) = 442 \pm 2 \pm 88$ nb/nucleon and a (model-dependent) total ψ' cross section $\sigma(p + N \to \psi' + X) = 75 \pm 5 \pm 22$ nb/nucleon. For J/ψ produced at central rapidity, $d\sigma(p + N \to J/\psi + X)/dy|_{y=0} = 230 \pm 5 \pm 46$ nb/nucleon.

I. INTRODUCTION

We report measurements of J/ψ and ψ' production in 800 GeV/c proton-gold collisions. Production of these charmonium states has been reported by previous experiments at various energies [1–3] and by our experiment at large x_F using copper and beryllium targets [4]. We compare our proton-gold results, obtained at small x_F, with these other measurements. Comparisons with leading-order QCD predictions are also presented, using recently-developed programs which calculate the inclusive distributions of quarkonium states produced in nucleon-nucleon collisions [5]. The programs are based upon quarkonium matrix elements calculated at leading order [6].

II. APPARATUS DESCRIPTION

A. Beam and Target

The experiment was performed at Fermilab using the upgraded E605 spectrometer [7]. The primary proton beam (typical intensity 6×10^{10} protons per 22 s spill) was incident along the z-axis upon the thin edge of a gold target of dimensions 5 cm $\times$ 200 μm $\times$ 3 mm ($\Delta x \times \Delta y \times \Delta z$). A scintillation-counter telescope viewing the target at 90° to the beam monitored the interaction rate. The telescope was calibrated at the beginning and end of the run against an ion chamber and a secondary-emission monitor (SEM) in the beam line by scanning the target vertically across the beam and recording the counts in the 90° telescope and the ion chamber at each position. The consistency of the calibrations before and after the run implies an rms uncertainty of 4% in the beam targeting fraction. Typically 60% of the beam intercepted the target, giving $\approx$ 50 MHz interaction rate. The SEM and ion chamber were calibrated by monitoring the production rate of ^{24}Na in copper foils, which were inserted into the beamline for special calibration runs, using the spallation cross sections of Baker *et al.* [8]. The stability of these calibrations, which have been repeated many times over the past decade, indicates an absolute uncertainty of 10% in the number of protons delivered by our beamline. The two effects in quadrature thus contribute 11% to the absolute normalization uncertainty.

B. Spectrometer

The primary goal of Fermilab Experiment 789 was to observe $J/\psi \rightarrow \mu^+\mu^-$ events arising from beauty decays downstream of the target. To separate the more copious direct-J/ψ production reported in this article from the rare beauty events [9], we installed a two-arm silicon-microstrip-detector (SMD) telescope (Fig. 1) downstream of the target. This vertex telescope, extending from 37 to 94 cm downstream of the target and covering vertical-angle ranges (+20 to +60) mr and (-20 to -60) mr in the laboratory, was used to reconstruct decay vertices occurring in or near the target. Each arm contained eight Micron Semiconductor "Type B" detectors, of dimensions 5 cm $\times$ 5 cm $\times$ 300 μm and 50-μm strip pitch; planes measuring the bend (y-z) view alternated with planes at $\pm 5°$ stereo angles.

The SMD telescope was followed by the Fermilab Meson-East spectrometer (Fig. 2). Charged particles emerging from the vicinity of the target were magnetically deflected around a beam dump suspended within the SM12 analysis magnet. The transverse-momentum kick of SM12 was 2.7 GeV/c. Particle trajectories were measured by three stations of small-cell drift chambers situated downstream of the SM12 magnet. The SM3 reanalysis magnet, with a 0.91 GeV/c transverse-momentum kick, provided a measurement of the particle momentum and confirmed the track origin. The ring-imaging Cherenkov counter (RICH) [10], electromagnetic and hadronic calorimeters, and muon detectors provided particle identification. (The RICH detector was not used in this analysis.) The muon detectors consisted of three proportional-tube planes and two hodoscope stations located behind thick absorber walls.

Tracks clearing the beam dump and within the fiducial region of the drift-chamber spectrometer occupied the vertical-production-angle ranges (+20 to +70) mr and (-20 to -70) mr, while the SMD telescopes were instrumented only to 60 mr. The prompt-J/ψ data were analyzed both with and without tracking requirements in the SMDs. The two methods were compared against Monte Carlo simulations in order to study and confirm our understanding of the geometrical acceptance. Both analyses gave consistent results. The analysis without SMD-track requirements yielded results over a slightly larger kinematic range in p_T and x_F and was used for the results presented here.

C. Trigger

For the data sample discussed here, the first-level trigger required a pattern of scintillation-hodoscope coincidences consistent with a pair of high-transverse-momentum muons originating in or near the target. The second-level trigger then required an opposite-sign pair of muon tracks. Fast lookup tables were employed in determining whether a set of hodoscope hits was consistent with a trajectory originating from the vicinity of the target. The trigger thus achieved substantial discrimination against muon pairs originating within the beam dump.

Further details concerning the apparatus, trigger, and analysis for another dimuon measurement using this spectrometer may be found in Moreno *et al.* [11].

III. DATA ANALYSIS

Including all triggers, approximately 10^9 events (of which $\approx 25\%$ were dimuon triggers) from 4×10^{13} interactions were recorded on 770 8-mm magnetic tapes. In the off-line analysis, events were reconstructed on four "farms" of Unix workstations at Fermilab. Each farm consisted of six 30 MIPS IBM or Silicon Graphics RISC workstations. Tracks reconstructed by the drift-chamber spectrometer were extrapolated to the target using the momentum determined by the SM3 analysis magnet. Tracks firing three of the five muon detectors were classified as muon tracks. The dimuon vertex determined from the extrapolated drift-chamber tracks was required to be within ± 25 cm of the target position in z. The known target position was then used to refine the parameters of each muon track. The resulting mass resolution for J/ψ mesons produced within the target was 16 MeV/c^2 rms. Monte Carlo studies (confirmed by data using the SMD-track analysis) indicate that this resolution

was dominated by multiple scattering of the muons in the target. The Monte Carlo program simulated multiple scattering and detector inefficiencies and used real event data to generate realistic noise hits in the detectors.

IV. RESULTS

Fig. 3 shows the mass spectrum of events identified as $\mu^+\mu^-$ pairs. The J/ψ and ψ' are observed on a smooth continuum arising from π and K decays in flight, the Drell-Yan process, and the semileptonic decays of heavy-quark hadrons. In each bin of p_T, x_F, or y, the continuum is fit with a polynomial or exponential form and subtracted from the data to extract the production rates of J/ψ and ψ' states.

Fig. 4 shows the invariant J/ψ production cross section times branching ratio versus the transverse momentum of the produced J/ψ. These per-nucleon cross sections have been determined using an atomic-weight (A) dependence of the form A^α with $\alpha = 0.90 \pm 0.02$ [12]. For the gold-target data presented here we neglect the small variation of α over our limited range in x_F and p_T. In addition to the errors shown there is a systematic normalization uncertainty of 20%. The main systematic errors are the uncertainties in luminosity ($\pm 11\%$), A dependence ($\pm 11\%$), trigger and reconstruction efficiency ($\pm 10\%$), fitting of the mass spectrum ($\pm 5\%$), and J/ψ branching ratio ($\pm 4\%$). We also estimate a point-to-point systematic uncertainty of 2%, attributed to small variations in hodoscope efficiencies and alignment; this has been added in quadrature with the statistical error of each point in all figures. Given our precise measurements of the x_F and p_T dependences of J/ψ production and the assumption of isotropic decay-angle distributions, we find the production-model dependence of the normalization to be negligible. Our results are compared in Fig. 4 with those of Clark *et al.* [1] obtained at the CERN ISR. At these center-of-mass energies, the production cross section in this central rapidity or small-x_F region appears to be relatively energy independent. The solid curve is a fit to our data using the functional form $A[1 + (p_T/B)^2]^{-6}$ where A and B are free parameters. The fit parameters are given in Table I.

Fig. 5 displays the differential J/ψ production cross section $d\sigma/dp_T^2$ per nucleon versus the transverse momentum of the produced J/ψ. These cross sections (listed in Table II) have been evaluated using the branching ratio $B(J/\psi \rightarrow \mu^+\mu^-) = (5.97 \pm 0.25)\%$ [13] and assuming the x_F shape $(1 - |x_F|)^5$ (see Table I and discussion below). For comparison, we show predictions (dashed curves), calculated at leading order in perturbative QCD, for the p_T distributions of J/ψ mesons originating from various quarkonium states [5]. The solid curve shows the sum of the quarkonium contributions. While the prediction and data show reasonable agreement in shape, the predictions have been increased by a "K factor" equal to 7 in order to get agreement in magnitude.

The QCD predictions are based on MRSD0 parton distributions [14]. They include the approximation of $z = 1$ fragmentation and decay, which implies that the transverse momentum of the J/ψ is the same as the transverse momentum of the quarkonium parent. The following branching ratios have been used: $B(\psi' \rightarrow J/\psi + X) = (57 \pm 4)\%$, $B(\chi_0 \rightarrow J/\psi + \gamma) = (0.66 \pm 0.10)\%$, $B(\chi_1 \rightarrow J/\psi + \gamma) = (27.3 \pm 1.6)\%$, $B(\chi_2 \rightarrow J/\psi + \gamma) = (13.5 \pm 1.1)\%$ [13]. Because the contributions from χ_0 and χ_2 resonances diverge at small p_T, an arbitrary p_T cutoff of 0.3 GeV/c is applied. These divergences are believed to be absorbed

by higher-order virtual contributions. We note that the exact value of the K factor needed to bring theory and experiment into agreement depends strongly on the choice of this cutoff, emphasizing the need for a higher-order calculation. Parton intrinsic transverse momentum (k_T) is simulated by adding a random Gaussian k_T kick of $< k_T^2 >= 0.5\,(\mathrm{GeV}/c)^2$ for each initial-state parton [15]; this is comparable to values derived from Drell-Yan studies [16].

Many previous predictions for J/ψ production have used the idea of semi-local duality [17,18]. In that model, the absolute normalization is a free parameter, due to the unknown fraction of produced $c\bar{c}$ pairs which hadronize as charmonium resonances. While the absolute normalization is not a free parameter for the prediction shown in Fig. 5, the large K factor needed shows that charm-quark production, or the charmonium hadronization fraction, is still not well understood. This discrepancy was noted by Baier and Rückl [6], who were able to accommodate the observed J/ψ yields only by using an abnormally large value of the QCD scale Λ ($\sim 500\,\mathrm{MeV}$).

Fig. 6 displays the differential ψ' production cross section $d\sigma/dp_T^2$ per nucleon versus the transverse momentum of the produced ψ'. These cross sections (listed in Table III) have been evaluated using the branching ratio $B(\psi' \to \mu^+\mu^-) = (0.77 \pm 0.17)\%$ [13] and assuming the same x_F shape as for the J/ψ. The J/ψ results are also displayed to show that while the ψ' data are consistent with the p_T shape observed for the J/ψ, there is a suggestion (at the level of 1.9 standard deviations; see Table I) that the ψ' p_T distribution is broader than that of the J/ψ. The normalization uncertainty of 30% is dominated by the branching-ratio uncertainty but does not include the large model dependence due to our assumed x_F shape. The leading-order prediction for ψ' production (smeared by intrinsic k_T) is shown in Fig. 6 rescaled by a K factor equal to 25. Large disagreements between data and theory for J/ψ and ψ' production have also been observed at $\sqrt{s} = 1.8\,\mathrm{TeV}$ [19].

Measurements of the J/ψ p_T distribution at other energies have been fit with either an exponential in p_T (Ae^{-Bp_T}) or an exponential in p_T^2 ($Ae^{-Bp_T^2}$). It was noted in Kaplan *et al.* [20] that the production of Drell-Yan dimuons is better characterized by a Gaussian-like behavior at small p_T and a power-law falloff for larger p_T, as in the functional form $A[1 + (p_T/B)^2]^{-6}$. The results of such fits to our data are given in Table I. The exponential forms in p_T or p_T^2 are not compatible with our J/ψ data, but all three forms give acceptable fits for the ψ'.

Fig. 7 displays the differential J/ψ and ψ' production cross sections $d\sigma/dx_F$ versus the fractional longitudinal momentum x_F of the produced meson in the nucleon-nucleon center-of-mass system. These per-nucleon cross sections (listed in Tables II and III) have been evaluated assuming the p_T shape $[1 + (p_T/B)^2]^{-6}$, with $B = 3\,\mathrm{GeV}/c$. The J/ψ data are well fit by a function of the form $A(1 - |x_F|)^B$ (see Table I). Also shown is a fit to the ψ' data using the same exponent as observed for the J/ψ, motivated by the ratio of ψ' to J/ψ production observed at large x_F [4], which agrees approximately with that observed here at small x_F; this is discussed further below. While the ψ' x_F dependence for $-0.03 < x_F < 0.15$ appears substantially flatter than that of the fit function, the fit is nevertheless acceptable (Table I).

The ratio of observed dimuon yields for J/ψ and ψ' is independent of the absolute normalization and the J/ψ and ψ' x_F and p_T dependences, and also is not subject to the 22% uncertainty in $B(\psi' \to \mu^+\mu^-)$. This ratio, evaluated in the ranges $-0.03 < x_F < 0.15$ and $0 < p_T < 2.5\,\mathrm{GeV}/c$, is displayed versus transverse momentum and Feynman x in Fig. 8.

We estimate the residual systematic uncertainty of this ratio at 10%. Averaging over p_T or x_F we find $B(\psi' \to \mu^+\mu^-) \times \sigma_{\psi'}/B(J/\psi \to \mu^+\mu^-) \times \sigma_{J/\psi} = 0.018 \pm 0.001 \pm 0.002$. This ratio is somewhat larger than that obtained at $x_F \approx 0.5$ [4] but consistent with values observed at $x_F = 0$ at $\sqrt{s} = 24$ and 27 GeV [21].

Our J/ψ data can be combined with large-x_F J/ψ cross-section measurements obtained from the copper beam dump in our apparatus [4,22] in order to form a more complete picture of J/ψ production over the full forward hemisphere. Fig. 9 displays the *per nucleus* differential J/ψ production cross section $d\sigma/dx_F$ for both data sets. The copper-beam-dump data have been converted to a per-nucleus cross section on gold by multiplying by $A_{\rm Au}(0.97 - 0.36\,x_F)$. This correction factor is a linear fit to our previous measurements of the x_F dependence of the ratio of heavy-nucleus to light-nucleus J/ψ production [4,23]. The solid curve shows a fit to the combined data using a function of the form $A(1 - |x_F|)^B$ (Table I). In determining the systematic error on the exponent we have included a relative normalization uncertainty of $\pm 15\%$ between the two data sets. This fit is in good agreement with the J/ψ fit shown in Fig. 7. While there is a discrepancy for the data points at $x_F = 0.325$ and $x_F = 0.375$, these are the points for which the systematic uncertainties in the beam-dump data are the largest [22]. The utility of this simple functional form over the full forward hemisphere and five decades in cross section is striking.

Fig. 10 displays the differential J/ψ production cross section $d\sigma/dy$ per nucleon versus the rapidity y of the produced meson. The cross sections are listed in Table IV. The solid curve shows a fit to the data using a function of the form $A(1 - |y|/6)^B$. We observe $d\sigma(p + N \to J/\psi + X)/dy|_{y=0} = 230 \pm 5 \pm 46$ nb/nucleon.

The functional forms for the x_F and p_T shapes can be used to infer total J/ψ and ψ' production cross sections. Using the differential cross section shown in Fig. 5, and integrating over $p_T > 2.5\,{\rm GeV}/c$ using the p_T shape $[1 + (p_T/B)^2]^{-6}$ with $B = 3\,{\rm GeV}/c$, we obtain $\sigma(p + N \to J/\psi + X) = 442 \pm 2 \pm 88$ nb/nucleon. As shown in Fig. 11, this cross section is consistent with previous measurements at other energies interpolated to our center-of-mass energy [1,24–29]. We have corrected the previous results for the current world-average value of $B(J/\psi \to \mu^+\mu^-)$ [13]. Where appropriate, we have converted $d\sigma/dy|_{y=0}$ measurements to total cross sections using $d\sigma/dy \simeq (2M_{J/\psi}/\sqrt{s})\,d\sigma/dx_F$ and the fit functional form shown in Fig. 9. The solid curve in Fig. 11 shows the result of a fit to all data using the functional form $Ae^{-B\sqrt{\tau}}$, where $\tau = M^2_{J/\psi}/s$. A preliminary total-cross-section measurement from another experiment [30] at the same energy as ours is also shown.

The value obtained for the total ψ' cross section is $\sigma(p + N \to \psi' + X) = 75 \pm 5 \pm 22$ nb/nucleon. This cross section is determined using the ψ' differential cross section shown in Fig. 6 and integrating over $p_T > 2\,{\rm GeV}/c$ using the same p_T shape as for the J/ψ. Since the x_F shape used, $d\sigma/dx_F \propto (1 - |x_F|)^5$, is not well determined for the ψ', the 30% systematic normalization uncertainty indicated should be considered a lower limit.

In summary, we have measured the J/ψ and ψ' production cross sections in $800\,{\rm GeV}/c$ proton-gold collisions. The J/ψ cross sections are in agreement with previous measurements. Leading-order QCD predictions for J/ψ and ψ' production give a good description of the shape of the data, but K factors equal to 7 for the J/ψ and 25 for the ψ' are necessary to reproduce the absolute normalization. These large K factors may reflect not only the absence of higher-order contributions in the calculation, but also possible contributions from other high-mass charmonium states not considered in the calculation [31], as well as from

components of the charmonium wave function [32] so far neglected. More data on both charmonium and bottomonium production at fixed-target and collider energies may be needed to identify the various contributions.

This work was supported by the U.S. Department of Energy and the National Science Foundation. KBL was partially supported by a DOE OJI award and an Alfred P. Sloan fellowship. YCC, GCK and PKT were supported by the National Science Council of the Republic of China. We thank the Fermilab staff for their support and M. L. Mangano for valuable discussions and assistance with the QCD predictions.

REFERENCES

[a] Present address: School of Physics and Astronomy, University of Minnesota, Minneapolis, MN 55455.

[b] Present address: Institute of Physics, Academia Sinica, Taipei, Taiwan, R.O.C.

[c] Present address: University of Mississippi, University, MS 38677.

[d] Present address: Science Applications International Corporation, 2950 Patrick Henry Drive, Santa Clara, CA 95054.

[e] Present address: Physics Department, Illinois Institute of Technology, Chicago, IL 60616.

[f] Present address: NASA/Goddard Space Flight Center, Greenbelt, MD 20771.

[g] Present address: Department of Physics, Iowa State University, Ames, IA 50011.

[1] A.G. Clark *et al.*, Nucl. Phys. **B142**, 29 (1978).

[2] L. Lyons, Prog. Part. Nucl. Phys. **7**, 169 (1981).

[3] L. Antoniazzi *et al.* Phys. Rev. D **46**, 4828 (1992).

[4] M. S. Kowitt *et al.*, Phys. Rev. Lett. **72**, 1318 (1994).

[5] M. L. Mangano,"Quarkonium Production Codes: Documentation."

[6] E. L. Berger and D. Jones, Phys. Rev. D **23**, 1521 (1981);
R. Baier and R. Rückl, Z. Phys. **C19**, 251 (1983);
B. Humpert, Phys. Lett. **184B**, 105 (1987);
R. Gastmans, W. Troost, and T. T. Wu, Nucl. Phys. **B291**, 731 (1987).

[7] Y. B. Hsiung *et al.*, Phys. Rev. Lett. **55**, 457 (1985);
J. A. Crittenden *et al.*, Phys. Rev. D **34**, 2584 (1986);
D. E. Jaffe *et al.*, Phys. Rev. D **40**, 2777 (1989).
For this run the SM0 magnet was removed, the six multiwire proportional chambers of Station 1 were replaced with small-cell drift chambers, and the data-acquisition system was upgraded to $\approx$1 Mbyte/s (50 Mbytes/spill) data-recording capability.

[8] S. I. Baker *et al.*, Nucl. Instrum. Meth. **222**, 467 (1984).

[9] D. M. Jansen *et al.*, Fermilab-Pub-94/403 (1994), to appear in Phys. Rev. Lett.

[10] P. B. Straub *et al.*, Phys. Rev. D **45**, 303 (1992) and references therein.

[11] G. Moreno *et al.*, Phys. Rev. D **43**, 2815 (1991).

[12] M. J. Leitch *et al.* (E789 collaboration), "Nuclear Dependence of J/ψ Production by 800 GeV/c Protons Near $x_F = 0$," Fermilab-Pub-95/047, submitted to Phys. Rev. D (1995).

[13] Particle Data Group, L. Montanet *et al.*, Phys. Rev. D **50**, Part 1 (1994).

[14] A. D. Martin, W. J. Stirling, and R. G. Roberts, Phys. Lett. B **306**, 145 (1993).

[15] M. L. Mangano, private communication.

[16] A. S. Ito *et al.*, Phys. Rev. D **23**, 604 (1981).

[17] H. Fritzsch, Phys. Lett. **67B**, 217 (1977).

[18] V. Barger, W. Y. Keung, and R. J. N. Phillips, Z. Phys. **C6**, 169 (1980).

[19] F. Abe *et al.* (CDF collaboration), Phys. Rev. Lett. **69**, 3704 (1992) and Fermilab-Conf-94/136-E (1994); E. Braaten *et al.*, Phys. Lett. B **333**, 548 (1994).

[20] D. M. Kaplan *et al.*, Phys. Rev. Lett. **40**, 435 (1978).

[21] H. D. Snyder *et al.*, Phys. Rev. Lett. **36**, 1415 (1976); B. C. Brown *et al.*, "Study of $J/\psi(3100)$ and $\psi(3700)$ Production in Proton-Nucleus Collisions with Electron and

Muon Pairs," Fermilab-Pub-77/54-EXP (1977).
[22] M. S. Kowitt, Ph.D. Thesis, Dept. of Physics, University of California at Berkeley, LBL-33331 (1992).
[23] D. M. Alde *et al.*, Phys. Rev. Lett. **66**, 133 (1991).
[24] K. J. Anderson *et al.*, Phys. Rev. Lett. **42**, 944 (1979).
[25] E. J. Siskind *et al.*, Phys. Rev. D **21**, 628 (1980).
[26] Yu. M. Antipov *et al.*, Phys. Lett. **60B**, 309 (1976).
[27] A. Bamberger *et al.*, Nucl. Phys. **B134**, 1 (1978).
[28] J. H. Cobb *et al.*, Phys. Lett. **68B**, 101 (1977).
[29] C. Kourkoumelis *et al.*, Phys. Lett. **91B**, 481 (1980).
[30] T. Alexopoulos *et al.*, "Production of J/ψ in 800 GeV/c p-Si Interactions," Fermilab-Conf-94/178-E.
[31] See e.g. F. E. Close, Phys. Lett. B **342**, 369 (1995); D. P. Roy and K. Sridhar, Phys. Lett. B **345**, 537 (1995); P. R. Page,"Excited Charmonium Decays by Flux-Tube Breaking and the ψ' Anomaly at CDF," OUTP-94-34-P, hep-ph@xxx.lanl.gov - 9502204 (1995).
[32] P. Cho and M. B. Wise, "Spin Symmetry Predictions for Heavy Quarkonia Alignment," CALT-68-1962, hep-ph@xxx.lanl.gov - 9411303; E. Braaten and S. Fleming, "Color-Octet Fragmentation and the ψ' Surplus at the Tevatron," NUHEP-TH-94-26, hep-ph@xxx.lanl.gov - 9411365 (1994).

TABLES

Meson	Fig.	Form	A	B	χ^2/NDF
J/ψ	4	$A[1+(p_T/B)^2]^{-6}$	$2.24 \pm 0.45\,\mathrm{nb}\,(\mathrm{GeV}/c)^{-2}$	$3.15 \pm 0.02\,\mathrm{GeV}/c$	2.8
J/ψ		$Ae^{-Bp_T^2}$	$234 \pm 47\,\mathrm{nb}\,(\mathrm{GeV}/c)^{-2}$	$0.55 \pm 0.01\,(\mathrm{GeV}/c)^{-2}$	5.0
J/ψ		Ae^{-Bp_T}	$366 \pm 73\,\mathrm{nb}\,(\mathrm{GeV}/c)^{-2}$	$1.21 \pm 0.01\,(\mathrm{GeV}/c)^{-1}$	30.0
J/ψ	6	$A[1+(p_T/B)^2]^{-6}$	$247 \pm 49\,\mathrm{nb}\,(\mathrm{GeV}/c)^{-2}$	$3.00 \pm 0.02\,\mathrm{GeV}/c$	2.8
ψ'		$Ae^{-Bp_T^2}$	$29.8 \pm 8.9\,\mathrm{nb}\,(\mathrm{GeV}/c)^{-2}$	$0.403 \pm 0.066\,(\mathrm{GeV}/c)^{-2}$	1.13
ψ'		Ae^{-Bp_T}	$41.8 \pm 12.5\,\mathrm{nb}\,(\mathrm{GeV}/c)^{-2}$	$0.84 \pm 0.11\,(\mathrm{GeV}/c)^{-1}$	0.57
ψ'	6	$A[1+(p_T/B)^2]^{-6}$	$30.7 \pm 9.2\,\mathrm{nb}\,(\mathrm{GeV}/c)^{-2}$	$3.60 \pm 0.32\,\mathrm{GeV}/c$	0.96
ψ'	7	$A(1-\lvert x_F\rvert)^B$	$184 \pm 55\,\mathrm{nb}$	5 (fixed)	1.7
ψ'		$A(1-\lvert x_F\rvert)^B$	$144 \pm 43\,\mathrm{nb}$	0.8 ± 1.4	0.3
J/ψ	7	$A(1-\lvert x_F\rvert)^B$	$1330 \pm 270\,\mathrm{nb}$	4.91 ± 0.18	0.75
J/ψ	9	$A(1-\lvert x_F\rvert)^B$	$158 \pm 32\ \mu\mathrm{b}$	5.09 ± 0.17	23
J/ψ	10	$A(1-\lvert y\rvert/6)^B$	$226 \pm 45\,\mathrm{nb}$	3.73 ± 0.20	0.44
J/ψ	11	$Ae^{-B\sqrt{\tau}}$	$1464 \pm 31\,\mathrm{nb}$	16.66 ± 0.12	45

TABLE I. Summary and comparison of fits to J/ψ and ψ' production cross sections. Errors include statistical and systematic uncertainties added in quadrature (see text).

x_F bin	$d\sigma/dx_F$ [nb/nucleon]	p_T bin	$d\sigma/dp_T^2$ [nb/(GeV/c)^2/nucleon]
		0.000 – 0.125	246.5 ± 8.1
-0.035 – -0.025	1247 ± 60	0.125 – 0.250	255.5 ± 6.5
-0.025 – -0.015	1221 ± 46	0.250 – 0.375	243.6 ± 5.9
-0.015 – -0.005	1235 ± 38	0.375 – 0.500	218.0 ± 5.2
-0.005 – 0.005	1316 ± 36	0.500 – 0.625	203.9 ± 4.9
0.005 – 0.015	1273 ± 33	0.625 – 0.750	171.8 ± 4.1
0.015 – 0.025	1168 ± 29	0.750 – 0.875	153.1 ± 3.8
0.025 – 0.035	1174 ± 28	0.875 – 1.000	137.3 ± 3.5
0.035 – 0.045	1076 ± 26	1.000 – 1.125	115.9 ± 3.0
0.045 – 0.055	1055 ± 25	1.125 – 1.250	106.2 ± 2.8
0.055 – 0.065	961 ± 23	1.250 – 1.375	86.0 ± 2.4
0.065 – 0.075	916 ± 22	1.375 – 1.500	73.0 ± 2.1
0.075 – 0.085	891 ± 22	1.500 – 1.625	61.1 ± 1.9
0.085 – 0.095	854 ± 22	1.625 – 1.750	45.7 ± 1.6
0.095 – 0.105	779 ± 22	1.750 – 1.875	41.6 ± 1.6
0.105 – 0.115	722 ± 24	1.875 – 2.000	33.6 ± 1.5
0.115 – 0.125	725 ± 30	2.000 – 2.125	23.9 ± 1.3
0.125 – 0.135	682 ± 38	2.125 – 2.250	21.4 ± 1.4
		2.250 – 2.375	13.3 ± 1.1
		2.375 – 2.500	11.6 ± 1.2
		2.500 – 2.625	8.5 ± 1.4

TABLE II. Differential cross sections for J/ψ production as functions of x_F and p_T. Errors are the quadrature sum of statistical and point-to-point-systematic uncertainties. There is an additional normalization uncertainty of 20%. These per-nucleon cross sections have been determined using $\sigma_A \propto A^\alpha$, with $\alpha = 0.90 \pm 0.02$.

x_F bin	$d\sigma/dx_F$ [nb/nucleon]	p_T bin	$d\sigma/dp_T^2$ [nb/(GeV/c)^2/nucleon]
		0.00 – 0.25	36.4 ± 6.8
-0.045 – -0.015	144 ± 56	0.25 – 0.50	29.9 ± 3.6
-0.015 – 0.015	151 ± 28	0.50 – 0.75	25.1 ± 3.1
0.015 – 0.045	137 ± 18	0.75 – 1.00	23.3 ± 2.8
0.045 – 0.075	135 ± 15	1.00 – 1.25	14.2 ± 2.4
0.075 – 0.105	132 ± 14	1.25 – 1.50	11.9 ± 2.4
0.105 – 0.135	148 ± 21	1.50 – 1.75	9.7 ± 2.5
0.135 – 0.165	98 ± 37	1.75 – 2.00	11.4 ± 2.4
		2.00 – 2.25	6.0 ± 2.5

TABLE III. Differential cross sections for ψ' production as functions of x_F and p_T. Errors are the quadrature sum of statistical and point-to-point-systematic uncertainties. There is an additional normalization uncertainty of at least 30% (see text). These per-nucleon cross sections have been determined using $\sigma_A \propto A^\alpha$, with $\alpha = 0.90 \pm 0.02$. $d\sigma/dx_F$ ($/dp_T^2$) contains an additional model dependence due to the assumed p_T (x_F) shape (see text).

y bin	$d\sigma/dy$ [nb/nucleon]	y bin	$d\sigma/dy$ [nb/nucleon]
-0.125 – -0.075	205.3 ± 7.6	0.325 – 0.375	178.1 ± 4.4
-0.075 – -0.025	219.0 ± 7.0	0.375 – 0.425	171.4 ± 4.2
-0.025 – 0.025	229.6 ± 6.6	0.425 – 0.475	168.5 ± 4.3
0.025 – 0.075	223.2 ± 6.1	0.475 – 0.525	165.0 ± 4.3
0.075 – 0.125	205.8 ± 5.3	0.525 – 0.575	157.6 ± 4.4
0.125 – 0.175	212.1 ± 5.3	0.575 – 0.625	156.0 ± 5.0
0.175 – 0.225	196.3 ± 4.9	0.625 – 0.675	147.2 ± 5.5
0.225 – 0.275	194.7 ± 4.8	0.675 – 0.725	140.7 ± 7.2
0.275 – 0.325	187.0 ± 4.6		

TABLE IV. Differential cross sections for J/ψ production vs. y. Errors are the quadrature sum of statistical and point-to-point-systematic uncertainties. There is an additional normalization uncertainty of 20%. These per-nucleon cross sections have been determined using $\sigma_A \propto A^\alpha$, with $\alpha = 0.90 \pm 0.02$.

FIGURES

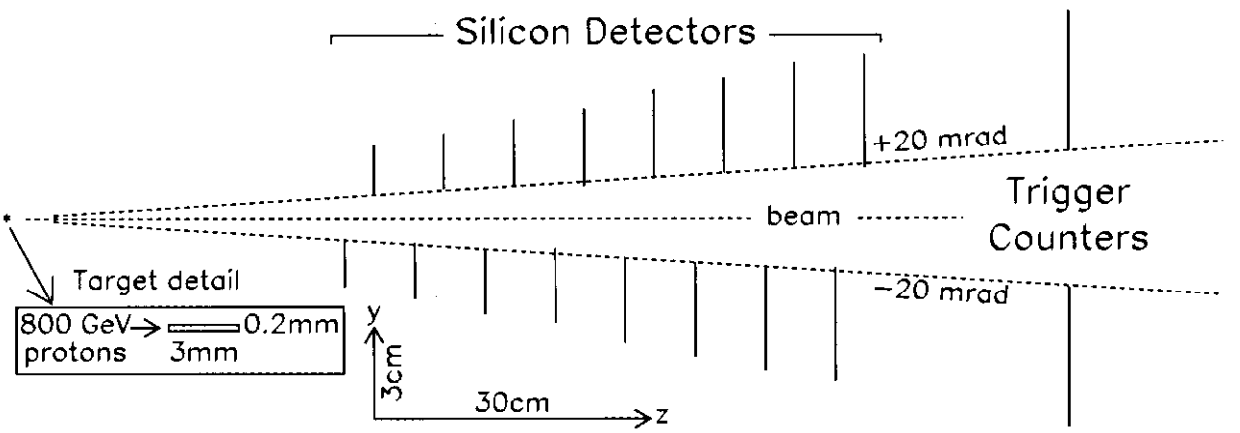

FIG. 1. Elevation view of E789 silicon vertex telescope.

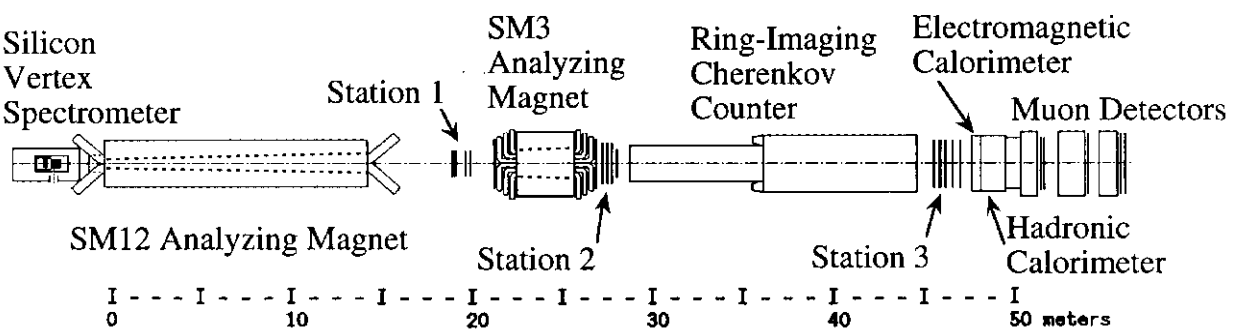

FIG. 2. Plan view of E789 spectrometer.

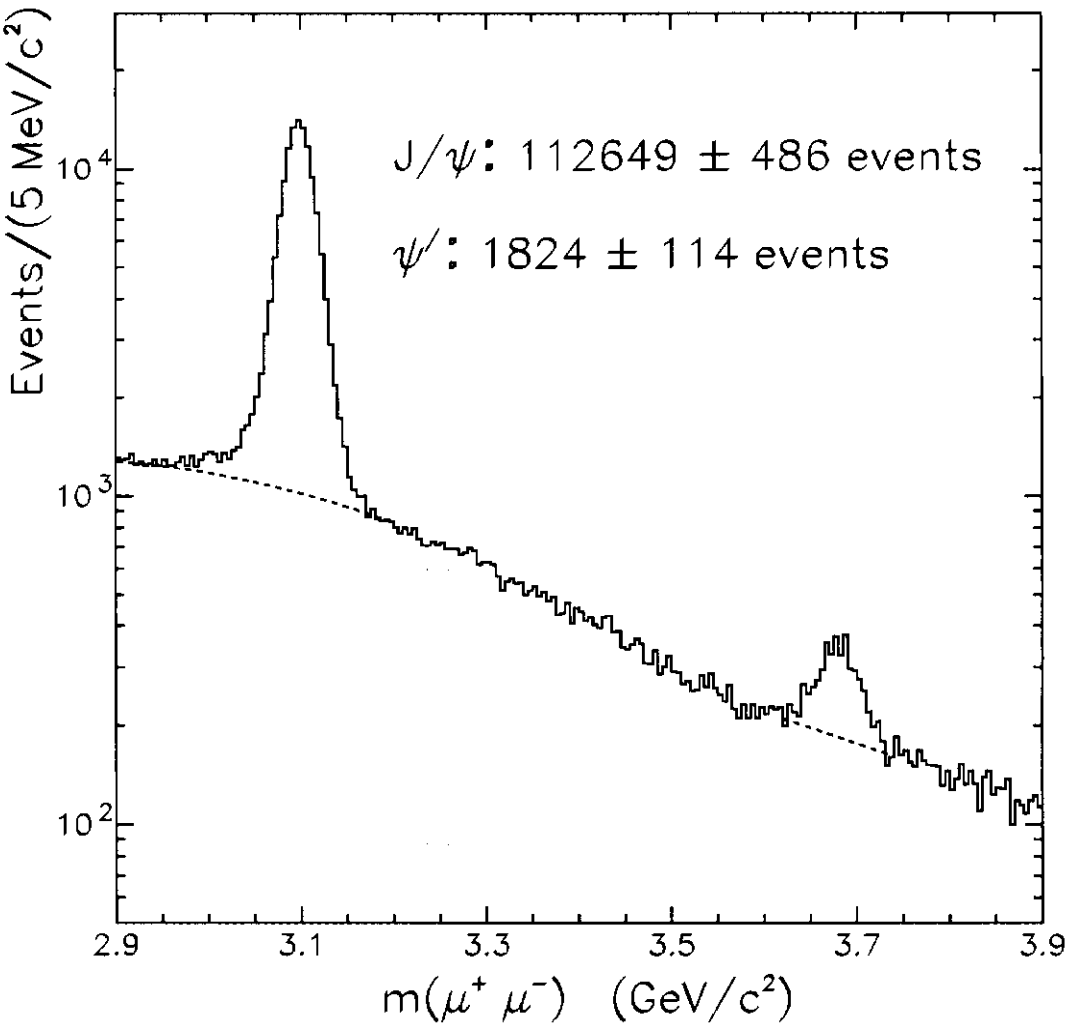

FIG. 3. Invariant-mass spectrum of events identified as $\mu^+\mu^-$ pairs. The dashed curves show the fits to the dimuon continuum under the J/ψ and ψ'.

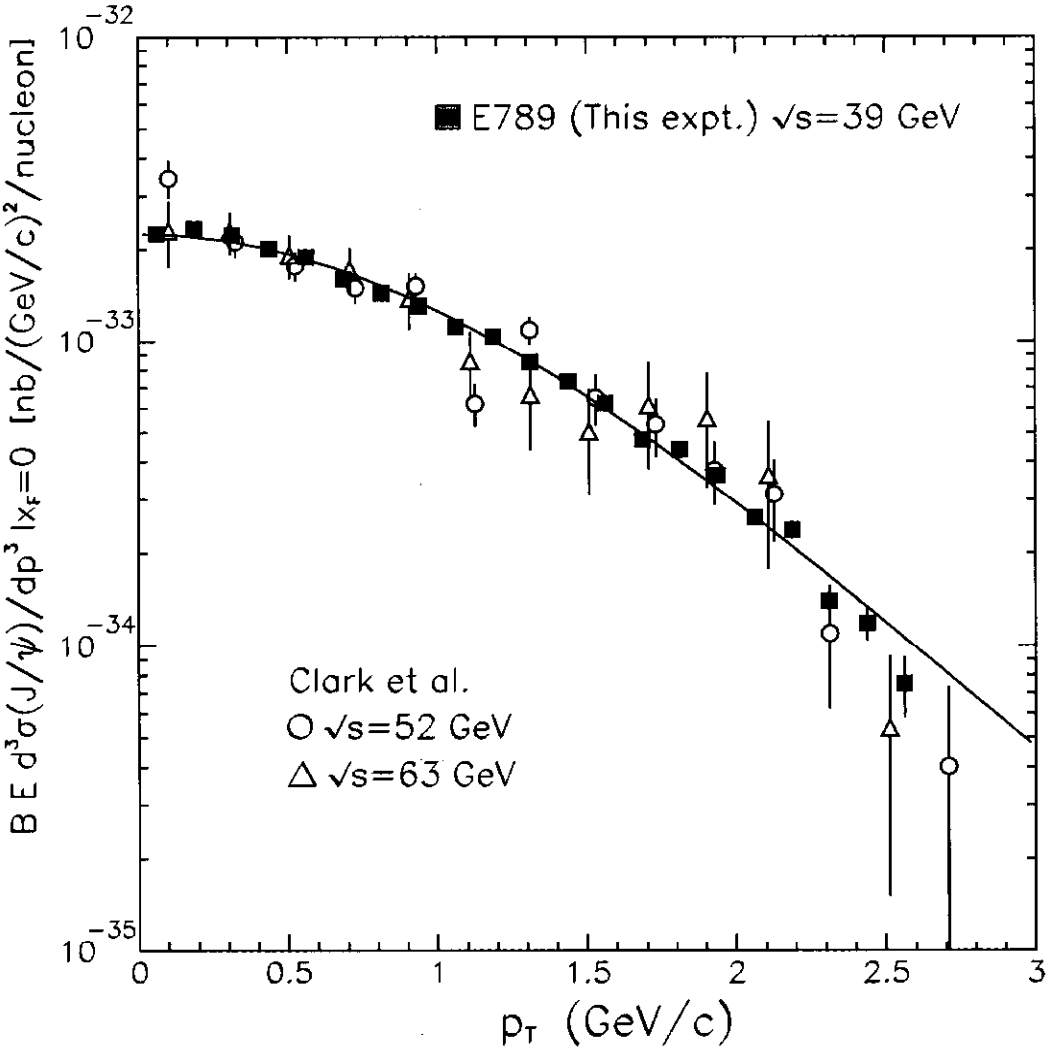

FIG. 4. Invariant cross section for J/ψ production versus the transverse momentum of the J/ψ. The 20% systematic normalization uncertainty is not shown. Our data are compared to results obtained at the CERN ISR [1]. A fit to our data, using the functional form $A[1+(p_T/B)^2]^{-6}$, is also shown.

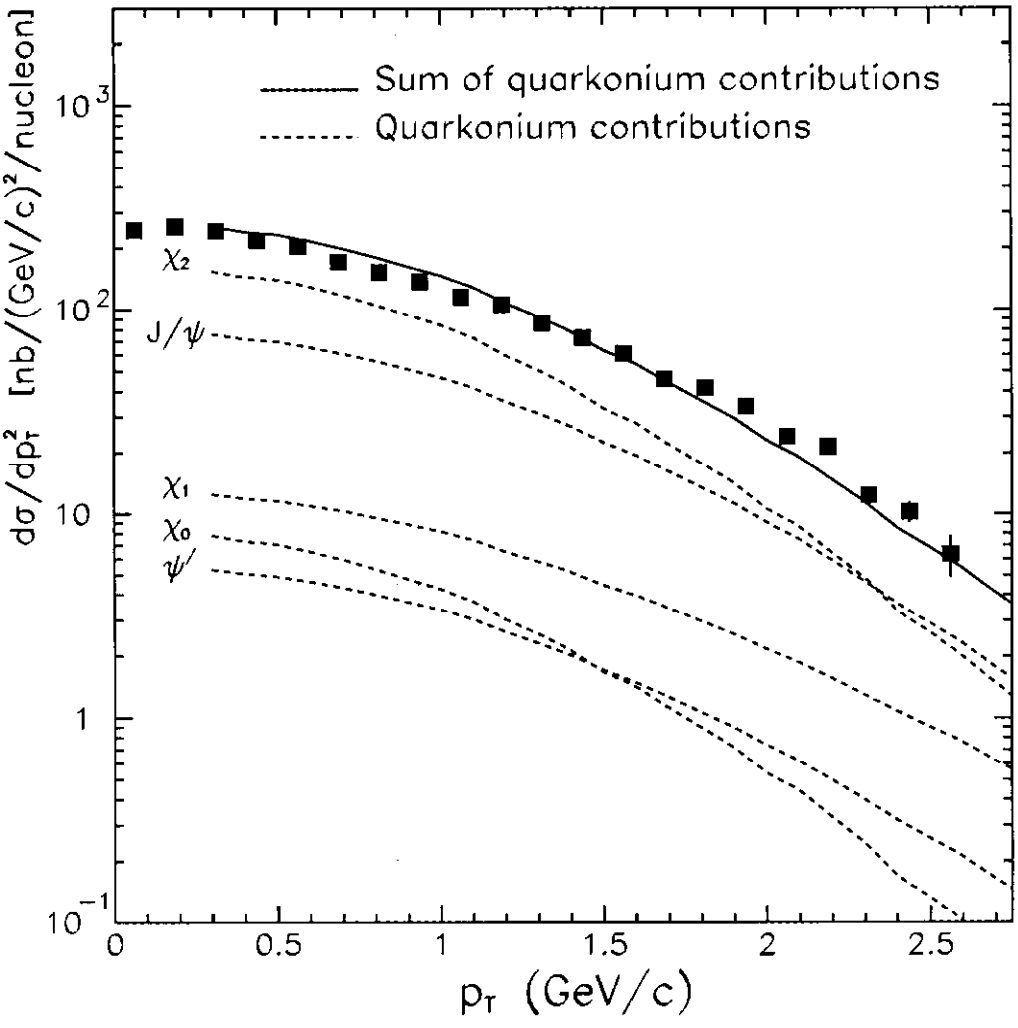

FIG. 5. Differential cross sections for J/ψ production versus the transverse momentum of the J/ψ. The 20% systematic normalization uncertainty is not shown. Leading-order predictions for the inclusive p_T distributions of quarkonium states, with K factors equal to 7, are also shown (dashed curves). The solid curve is the sum of the quarkonium contributions. See text for details.

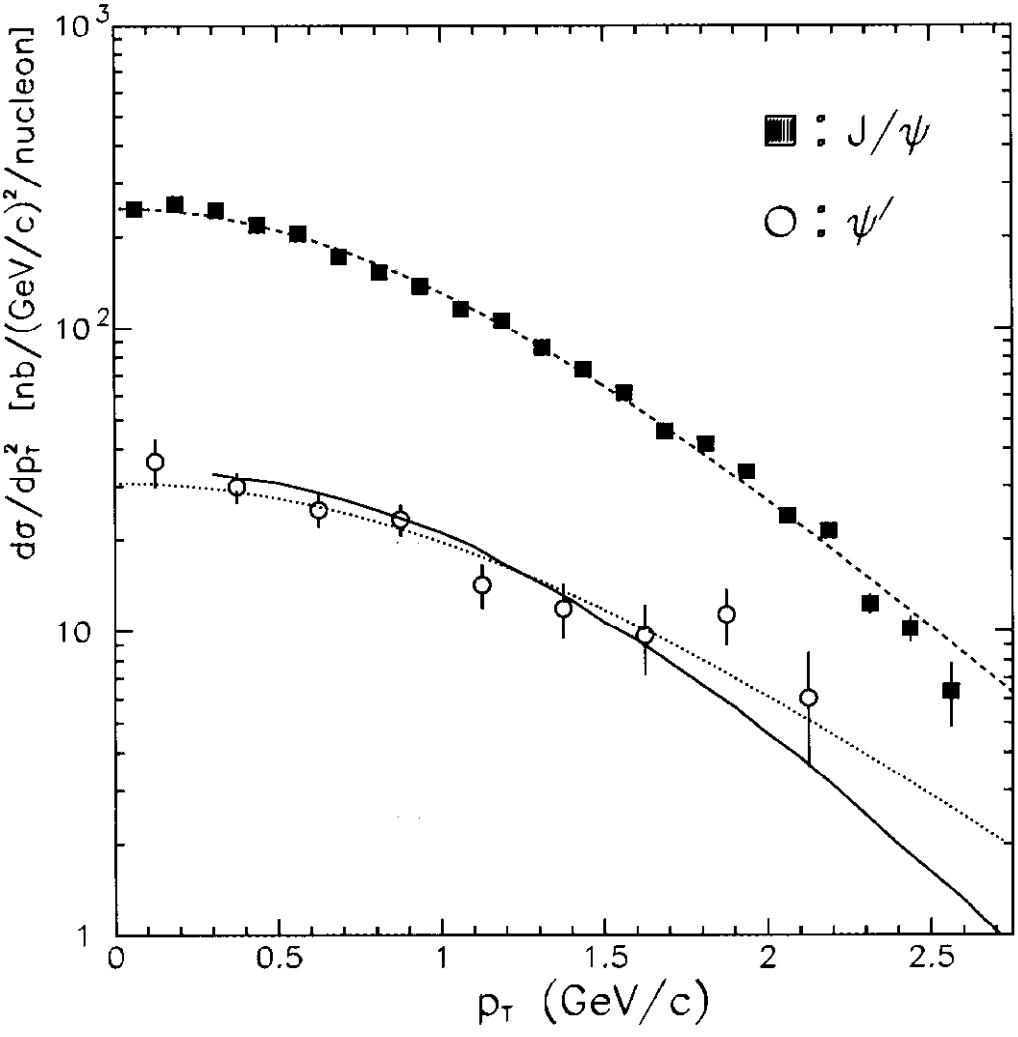

FIG. 6. Differential cross sections for J/ψ and ψ' production versus the transverse momentum of the meson. The 20% (30%) systematic normalization uncertainty for the J/ψ (ψ') is not shown. Note that $d\sigma/dp_T^2$ for the ψ' contains an additional model dependence due to the assumed x_F shape (see text). The leading-order prediction for the inclusive p_T distribution of ψ' mesons, with a K factor equal to 25, is also shown (solid curve). The dashed and dotted curves are fits to the data using the functional form $A[1 + (p_T/B)^2]^{-6}$.

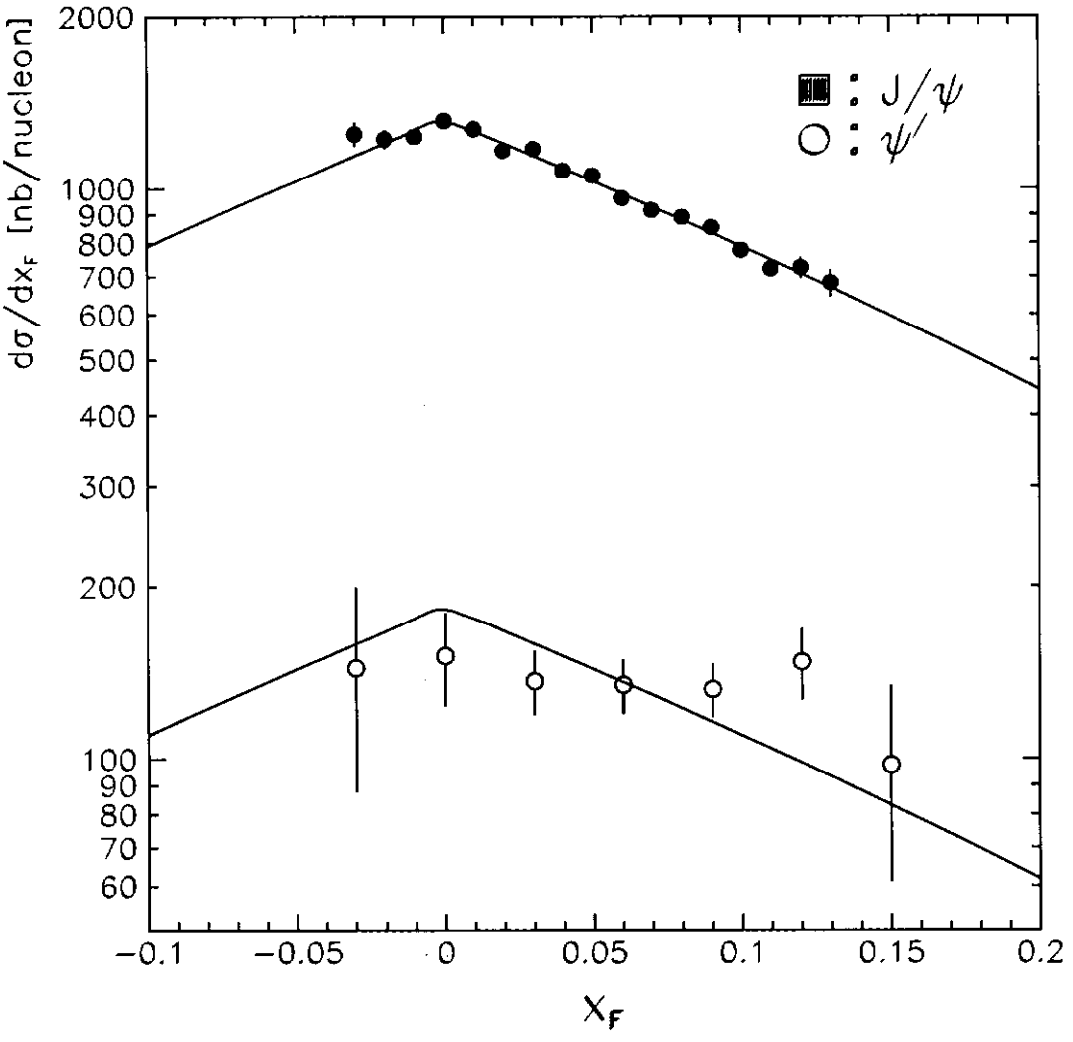

FIG. 7. Differential cross section for J/ψ and ψ' production versus x_F. The 20% (30%) systematic normalization uncertainty for the J/ψ (ψ') is not shown. Note that $d\sigma/dx_F$ for the ψ' contains an additional model dependence due to the assumed p_T shape (see text). For the J/ψ, the solid curve is a fit to the data using the functional form $A(1-|x_F|)^B$. For the ψ', the solid curve shows the result of a fit using the same exponent as observed for the J/ψ.

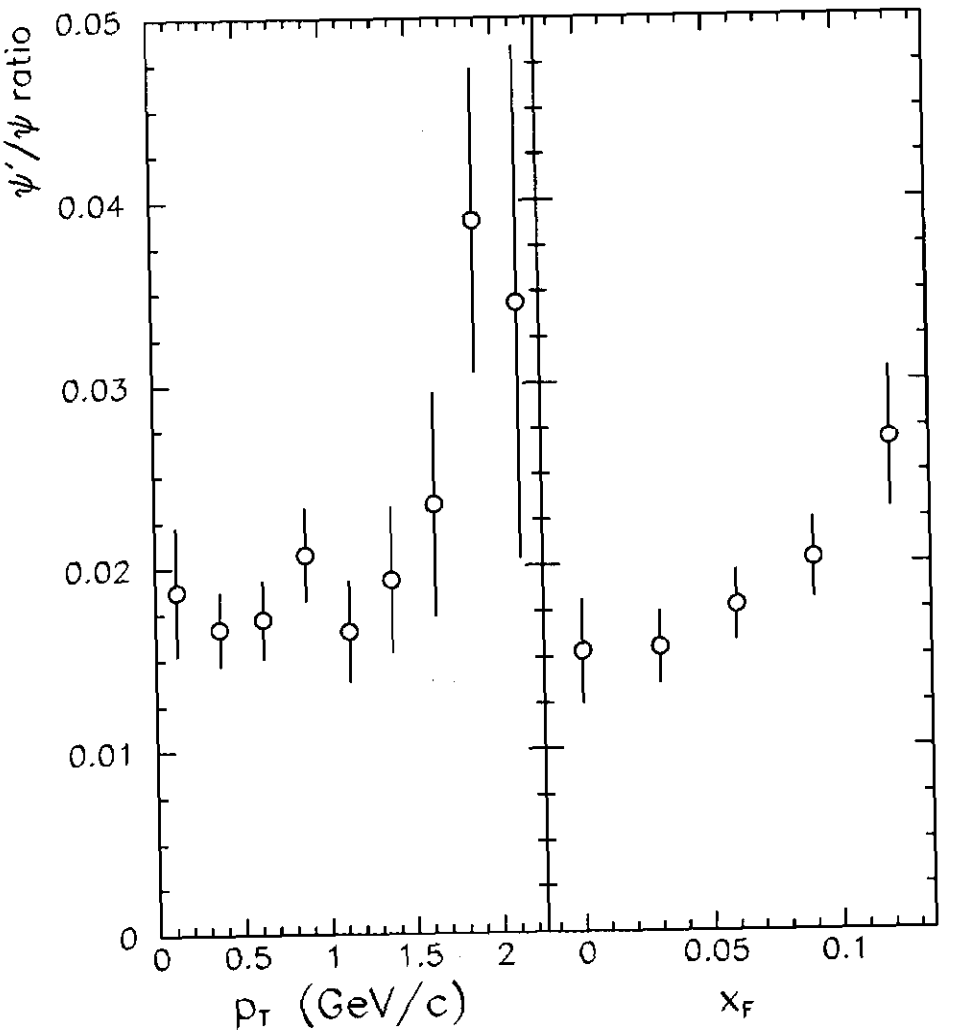

FIG. 8. Observed ratio of yields for $\psi' \to \mu^+\mu^-$ and $J/\psi \to \mu^+\mu^-$ versus p_T for the bin $-0.03 < x_F < 0.15$ and versus x_F for the bin $0 < p_T < 2.5\,\mathrm{GeV}/c$.

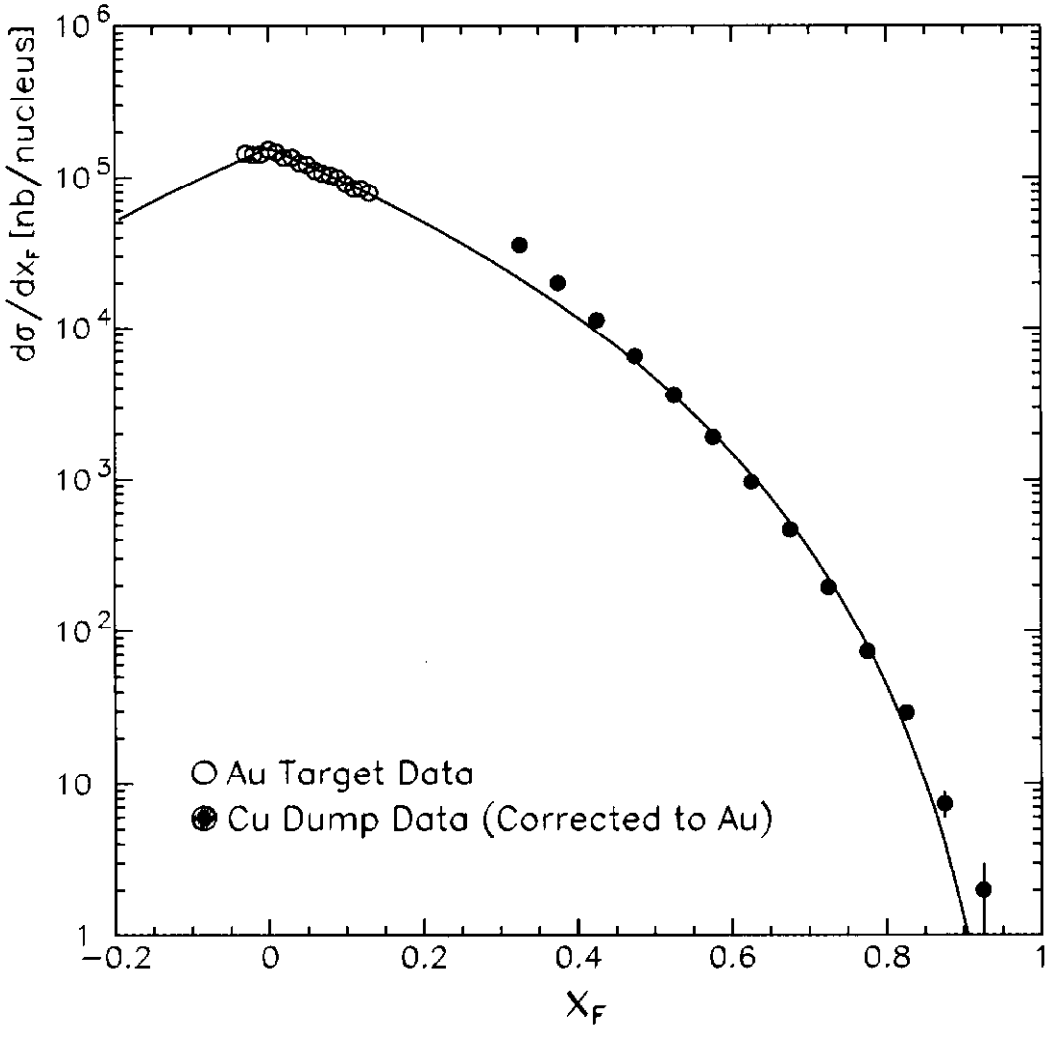

FIG. 9. Differential cross section for J/ψ production versus x_F. Data from the copper beam dump [4,22] and the gold target are shown. The solid curve is a fit to the data using the functional form $A(1-|x_F|)^B$.

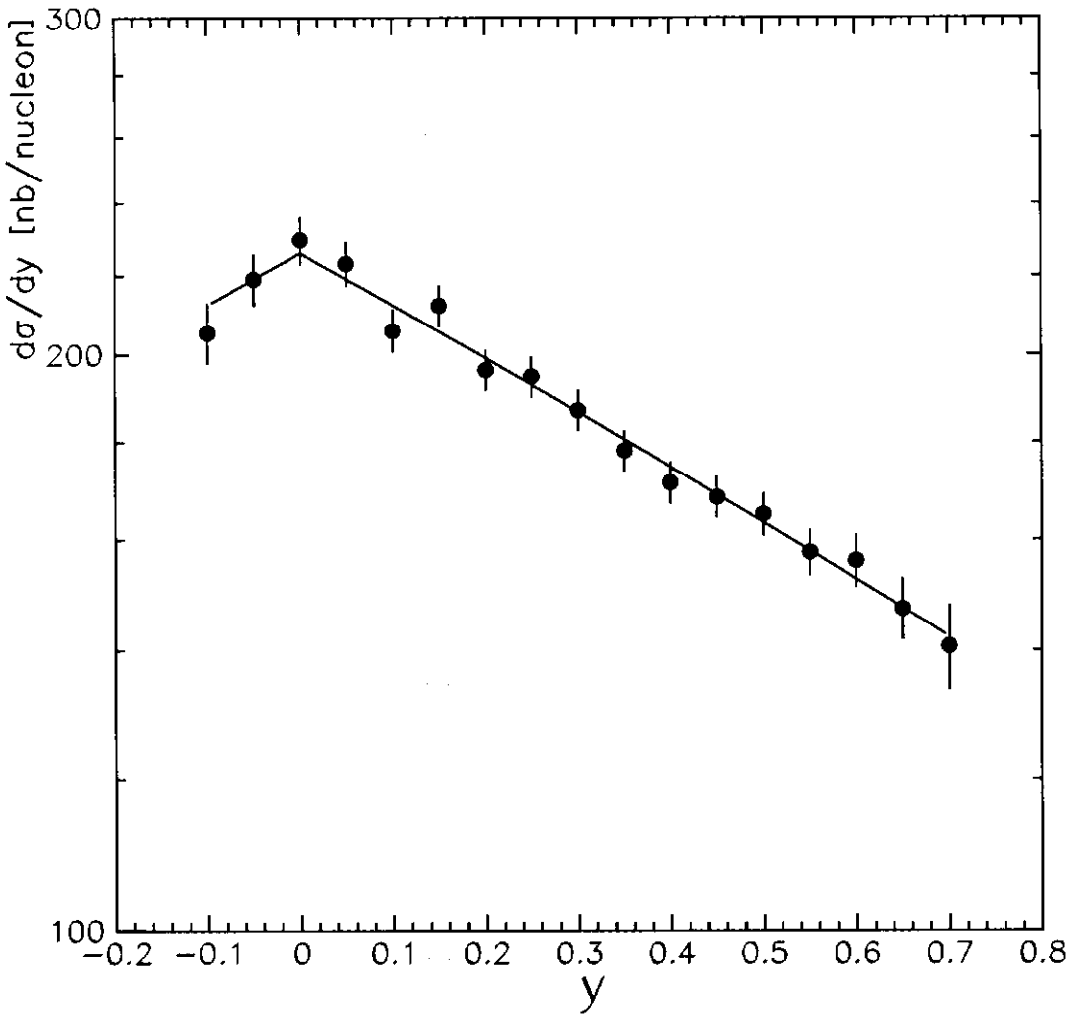

FIG. 10. Differential cross section for J/ψ production versus rapidity. The solid curve is a fit to the data using the functional form $A(1-|y|)^B$.

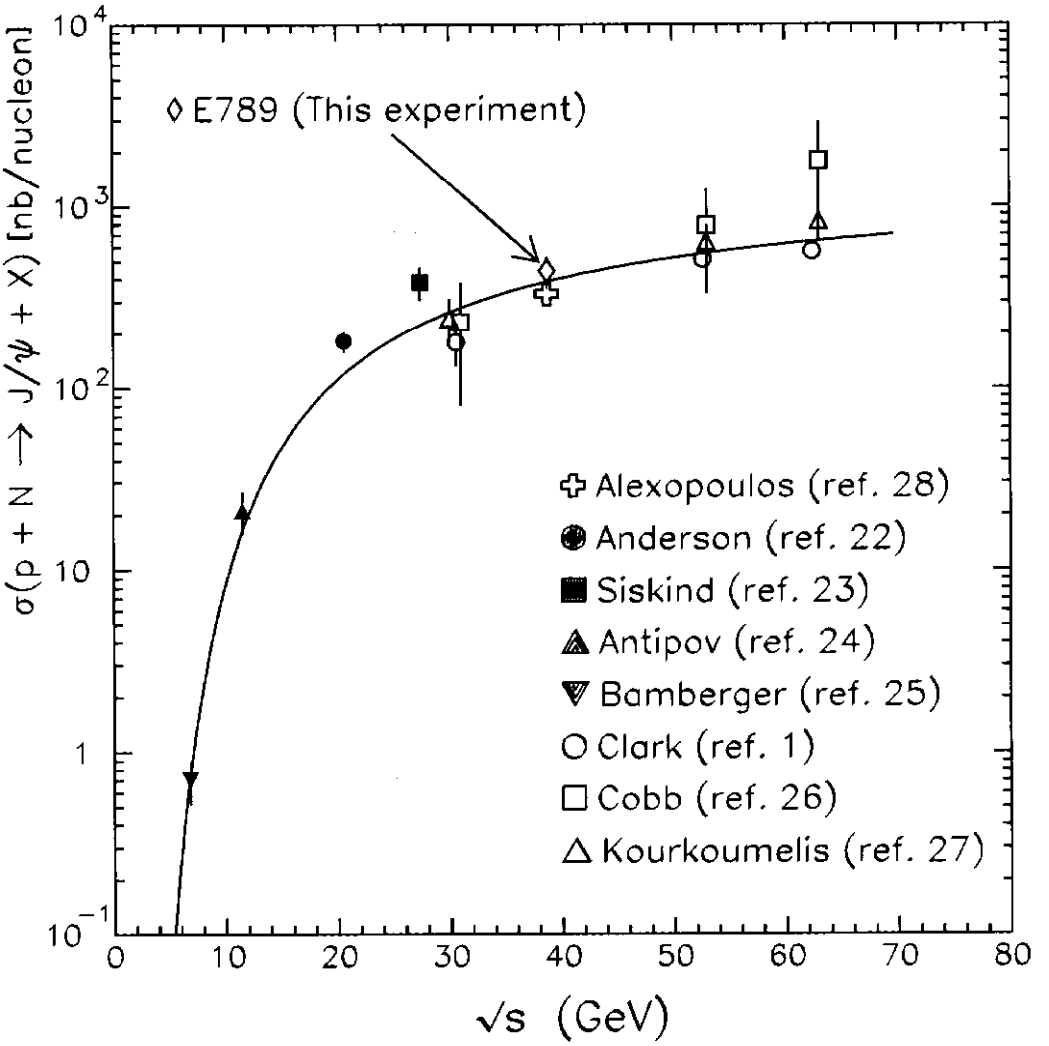

FIG. 11. Total cross section for J/ψ production versus center-of-mass energy. The solid curve is a fit to the data using the functional form $Ae^{-B\sqrt{\tau}}$ where $\tau = M^2_{J/\psi}/s$. See text for details.